INTERNATIONAL JOURNAL FOR NUMERICAL METHODS IN FLUIDS
Int. J. Numer. Meth. Fluids 2010; **63**:743–768
Published online 22 June 2009 in Wiley InterScience (www.interscience.wiley.com). DOI: 10.1002/fld.2100

QALE-FEM for modelling 3D overturning waves

S. Yan and Q. W. Ma*, †

School of Engineering and Mathematical Sciences, City University, London EC1V 0HB, U.K.

SUMMARY

A further development of the QALE-FEM (quasi-arbitrary Lagrangian–Eulerian finite element method) based on a fully nonlinear potential theory is presented in this paper. This development enables the QALE-FEM to deal with three-dimensional (3D) overturning waves over complex seabeds, which have not been considered since the method was devised by the authors of this paper in their previous works (*J. Comput. Phys.* 2006; **212**:52–72; *J. Numer. Meth. Engng* 2009; **78**:713–756). In order to tackle challenges associated with 3D overturning waves, two new numerical techniques are suggested. They are the techniques for moving the mesh and for calculating the fluid velocity near overturning jets, respectively. The developed method is validated by comparing its numerical results with experimental data and results from other numerical methods available in the literature. Good agreement is achieved. The computational efficiency of this method is also investigated for this kind of wave, which shows that the QALE-FEM can be many times faster than other methods based on the same theory. Furthermore, 3D overturning waves propagating over a non-symmetrical seabed or multiple reefs are simulated using the method. Some of these results have not been found elsewhere to the best of our knowledge. Copyright © 2009 John Wiley & Sons, Ltd.

Received 24 October 2008; Revised 26 March 2009; Accepted 4 May 2009

KEY WORDS: QALE-FEM; 3D overturning waves; spring analogy method; complex seabed; fully nonlinear potential flow; fully nonlinear waves; potential theory for waves

1. INTRODUCTION

Overturning waves are common physical phenomena in the sea, particularly in the nearshore area. The destructive energy released by overturning waves may result in huge loads and cause severe damage. For example, the overturning wave in the 2004 Great Sumatra Tsunami caused collapse of numerous buildings and death of many people [1]. In order to reduce the losses due to such events, many efforts, e.g. building submerged breakwaters/artificial reefs to protect the beach [2], have

*Correspondence to: Q. W. Ma, School of Engineering and Mathematical Sciences, City University, London EC1V 0HB, U.K.
†E-mail: q.ma@city.ac.uk

Contract/grant sponsor: Leverhulme Trust, U.K.; contract/grant number: F/00353/G

been and are still being made. The effectiveness of these efforts depends on a good understanding of overturning waves. Owing to the strong nonlinearity, the linear, second-order or higher-order approximate solutions (see, for example [3–5]) may not be sufficient to describe overturning waves. This initiates an interest in fully nonlinear numerical simulation of these waves. For this purpose, two classes of mathematical models have been employed, as summarized below.

The first one is called the Navier–Stokes (NS) Model, in which the NS equation and the continuity equation (or equivalent pressure Poisson equation, see [6]) together with proper boundary conditions are solved using numerical methods. These numerical methods may be split into two groups: conventional mesh-based methods and meshless methods. The former mainly includes the finite volume method [7–12], finite difference method [13] and cubic interpolated propagation method [14]. The latter covers smoothed particle hydrodynamic [15–17], moving particle semi-implicit method [18, 19] and particle finite element method [20]. However, no matter which method is used, solving NS equations is always a time-consuming task, particularly for three-dimensional (3D) cases. For more reviews on the NS Model, readers may be referred to the above cited papers.

The second one is called FNPT model, in which a Laplace's equation for velocity potential with fully nonlinear boundary conditions is dealt with. Compared with the NS model, the number of variables as well as the complexity of the governing equations in this model is dramatically decreased. As a result, the FNPT model needs much less computational resources than the NS model and, therefore, is computationally much more efficient. Although viscosity is ignored in the FNPT model, comparison with experimental data [6, 21–25] has shown that the results obtained by using this model are sufficiently accurate for strong nonlinear waves up to overturning. Other comparison between the FNPT model and the finite-volume-based NS model has also revealed that the results from the former are closer to experimental data than those from the latter in the cases with non-breaking overturning solitary waves [26, 27]. The reason may be that the finite-volume-based NS model suffers from numerical diffusion, leading to energy loss over a long distance of wave propagation, as indicated by Grilli *et al*. [28]. Therefore, the FNPT model is preferred over the NS model in terms of both computational efficiency and accuracy, unless post-breaking waves, i.e. after the overturning jet hits the free surface, are of main concern. In addition, a coupled FNPT-NS model has recently been developed and applied to simulate 2D breaking waves [29, 30]. In this kind of model, the FNPT model is used to simulate the pre-breaking wave while the NS model continues the calculation in the post-breaking stage.

This paper aims to present a method simulating 3D overturning waves, excluding the post-breaking stage, thus the FNPT model is chosen. The problems formulated by the FNPT model are usually solved by a time-marching procedure. In this procedure, the key task is to solve a boundary value problem (BVP) by using a numerical method, e.g. boundary element method (BEM) or finite element method (FEM). A brief review on this model for simulating nonlinear water waves without overturning has been given by Ma and Yan [21]. Only the references related to overturning waves are discussed here. The application of the FNPT model to numerically model overturning waves can be traced back to Longuet-Higgins and Cokelet [31]. The earlier researchers focused on 2D problems with a relatively simple computational domain, i.e. in deep water [32] and/or in a spatially periodic domain [33, 34]. However, in the real sea, the seabed effects could be very evident and the spatially periodic problems are rare to see. In later 2D studies, these limitations on the fluid domain and on the water depth were removed [35–46]. The waves in these applications include propagating oscillating waves (see, for example [44, 46]), solitary waves (see, for instance [39, 41]) and wave groups [40, 45]. Apart from them, Zhao and Faltinsen [47] studied overturning waves initiated by water entry of 2D bodies and Grilli and Subramanya [22] investigated 2D

DOI: 10.1002/fld

overturning waves generated by moving boundaries. 2D overturning waves are not the focus of this paper. Reader may be referred to the cited papers above for more literature about them.

Compared with 2D overturning waves, numerical simulation of 3D overturning waves requires much more computational resource and sophisticated techniques. Owing to this, the applications of the FNPT model to 3D overturning waves are still rare. Xü and Yue [48, 49] modelled 3D overturning Stokes waves in space–periodic numerical tank. In their model, the waves are generated by specifying pressure distributions on the free surface. This model has been extended by Xue *et al*. [50] to simulate crescent waves in water of infinite depth, which are generated by specifying initial wave elevation and the velocity potential on the free surface based on a linear theory, again in a spatially periodic domain. Grilli *et al*. [28] developed another FNPT-based model for 3D overturning waves in water of finite depth. Guyenne and Grilli [51] followed the work and investigated the effect of seabeds on overturning solitary waves. By using this model, Grilli *et al*. [52] simulated 3D tsunami waves generated by underwater landslides and Brandini and Grilli [53] modelled 3D overturning freak waves over a flat seabed. Although these applications have shown a good applicability of this model, its computational efficiency needs to be improved. For this purpose, Fochesato and Dias [54] introduced a fast multipole algorithm, referred as fast BEM method. The fast BEM method has successfully modelled 3D overturning solitary waves [54] and freak waves [55]. Their numerical tests indicated that the fast BEM method can be 6 times faster than the conventional BEM by Grilli *et al*. [28]. It could be considered as the fastest method at the time for modelling 3D overturning waves. Although these methods show less limitation on the wave generation and seabed geometries than those models based on infinite water depth and periodical domain, it has not been used to investigate overturning of propagating oscillating waves, which are more popular than solitary waves or freak waves in reality. In addition, the seabed geometry in their applications is symmetrical about the central longitudinal vertical plane, a special case of real seabed geometry. More investigations on other types of waves and non-symmetrical seabed are interesting.

In the studies discussed above, the BVP is solved by using the BEM, either linear/low-order BEM (see, for instance [44]), higher-order BEM (see, for example [28]) or the fast BEM [54, 55]. On the other hand, the FEM has been developed by Wu and Eatock Taylor [56] and Ma *et al*. [57, 58] to solve fully nonlinear wave problems. As pointed out by them, the FEM requires less memory and is therefore computationally more efficient for fully nonlinear waves than the BEM, which will be confirmed again in this paper. However, for the FEM, a good computational mesh (good element shapes and reasonable node distribution), covering the whole fluid domain, is required and needs to be updated at every time step in order to conform to the motion of the free surface. For the problems where the free surface is always single valued, i.e. without wave overturning, one may use a structured mesh (for example [57, 58]), which needs a little CPU time to be updated or regenerated. However, once overturning waves occur, an unstructured mesh (at least near the overturning jet) is necessary to achieve accurate results. Repeatedly regenerating such a mesh may take a major part of CPU time and so make the overall simulation very slow. To reduce the CPU time spent on regenerating a suitable mesh, one may use a hybrid structured–unstructured mesh, which is unstructured near the overturning jet and structured in the other region, as adopted by Turnbull *et al*. [59] and Heinze [60] for 2D wave–structure interaction problems without overturning. But this technique still needs to regenerate the unstructured part and needs to know where the overturning occurs *a priori*. Apart from the challenge associated with the mesh, it is crucial to use a robust method to evaluate the fluid velocities on the free surface because they are needed to update the information on the free surface at every time step. Several methods for this purpose have been

DOI: 10.1002/fld

developed in the FEM. They mainly include the direct method (solving the velocity in a similar way to the velocity potential) developed by Wu and Eatock Taylor [56] and followed by Wang and Wu [61], Wang *et al*. [62], the finite difference method [63, 64], the three-point method suggested by Ma *et al*. [57] (see also [65]) and the cubic spline method suggested by Sriram *et al*. [66]. Only the direct method and the three-point method have been employed for 3D nonlinear water waves in those papers. The three-point method has been proved more robust and accurate than the former. However, this method is originally developed for meshes with special structures, i.e. at least two nodes lying on the vertical line through each free-surface node, which is hard to be satisfied when using unstructured meshes. Perhaps due to these two challenges, i.e. regenerating arbitrary unstructured meshes and evaluating the fluid velocities, the conventional FEM has not been demonstrated to model overturning waves, even in 2D cases. Ma and Yan [21] have recently devised a new method called QALE-FEM (quasi-arbitrary Lagrangian–Eulerian finite element method). In this method the complex unstructured mesh is generated only once at the beginning of the calculation and is moved at other time steps to conform to motions of boundaries by using a novel and robust spring analogy method purpose-developed for water waves. This feature allows one to use an unstructured mesh with any degree of complexity without the need of regenerating it. Furthermore, a velocity calculation method suitable for the arbitrary moving unstructured meshes is also developed based on the three-point method. The QALE-FEM has been successfully used to simulate nonlinear waves and its interactions with complicated seabeds [21, 25, 67] and free responses of floating bodies to steep waves [68–70]. Ma and Yan [21] compared the QALE-FEM with the conventional FEM in terms of computational efficiency and accuracy in the cases for periodic bars on the seabed. They concluded that the QALE-FEM may require less than 15% of the CPU time required by the conventional FEM to achieve the same level of accuracy.

In this paper, the QALE-FEM is extended to simulate 3D overturning waves before the overturning jet hits the free surface ahead of the wave. In order to tackle the challenges associated with overturning waves, two new numerical techniques are developed. These include special techniques for moving mesh and for evaluating the fluid velocity in the cases for 3D overturning waves. The accuracy of the QALE-FEM with the newly developed techniques is studied by comparing the numerical results with experimental data and other results available in the public domain. Good agreement is achieved. The convergent property and the computational efficiency are also investigated. Based on these, numerical investigations on solitary waves over a 3D non-symmetrical sloping seabed and transient oscillating waves propagating over artificial reefs, which have not been made before to the best of our knowledge, are presented.

2. MATHEMATICAL MODEL

In this paper, the computational domain is chosen as a rectangular tank. Two types of methods are used to generate nonlinear waves. The first one is to utilize a piston or paddle wavemaker which is mounted at the left end of the tank (see Figure 1). The second one is to specify the initial condition for the position of and the velocity potential on the free surface. In this case, the wavemaker shown in Figure 1 is treated as a fixed boundary. Reflective boundary conditions are implemented on the lateral boundaries while the absorbing boundary condition is applied at the right end of the tank unless mentioned otherwise. For the absorbing boundary condition, a damping zone with a Sommerfeld condition is applied, as sketched in Figure 1. Details can be found in [57]. Arbitrary forms of seabed geometry may appear. A Cartesian coordinate system is adopted with the *oxy* on

DOI: 10.1002/fld

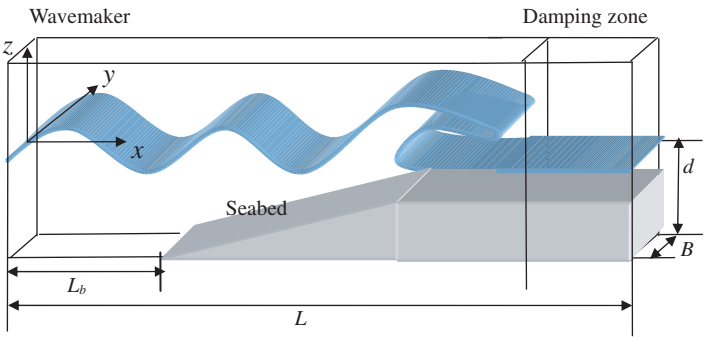

Figure 1. Sketch of fluid domain.

the mean free surface, the *oxz* coinciding with the central longitudinal vertical plane of the tank and the z-axis being positive upwards.

Similar to the usual formulation for the FNPT Model, the velocity potential (ϕ) satisfies Laplace's equation

$$\nabla^2\phi = 0 \tag{1}$$

in the fluid domain. On the free surface $z=\zeta(x, y, t)$, the velocity potential satisfies the kinematic and dynamic conditions in the following Lagrangian form:

$$\frac{Dx}{Dt}=\frac{\partial\phi}{\partial x}, \quad \frac{Dy}{Dt}=\frac{\partial\phi}{\partial y}, \quad \frac{Dz}{Dt}=\frac{\partial\phi}{\partial z} \tag{2}$$

$$\frac{D\phi}{Dt}=-gz+\frac{1}{2}|\nabla\phi|^2 \tag{3}$$

where (D/Dt) is the substantial (or total time) derivative following fluid particles and g is the gravitational acceleration. In Equation (3), the atmospheric pressure has been taken as zero. On all rigid boundaries, such as the wavemaker, the velocity potential satisfies

$$\frac{\partial\phi}{\partial n}=\mathbf{n}\cdot\mathbf{U}(t) \tag{4}$$

where $\mathbf{U}(t)$ and $\mathbf{n}$ are the velocity and the outward unit normal vector of the rigid boundaries, respectively.

The problem described by Equations (1)–(4) is solved by using a time-step-marching procedure. At each time step, the BVP for the velocity potential is solved by the FEM. The details about the FEM formulation have been described in our previous publications [21, 57] and will not be repeated here.

3. SUMMARY OF THE QALE-FEM

As indicated in the Introduction, the QALE-FEM devised by Ma and Yan [21] will be further developed in this paper to deal with 3D overturning waves. This method for problems about waves

DOI: 10.1002/fld

without floating bodies includes two key elements in comparison with the conventional FEM method presented in [57]: (1) the scheme for moving mesh and (2) the method for estimating the fluid velocity on the free surface. All the elements have been described in [21]. For completeness, the two elements presented in our previous related papers will be summarized in the next two sub-sections before presenting new developments.

3.1. Scheme for moving mesh

In the QALE-FEM, the computational mesh is generated only once at the beginning of the calculation and is moved at other time steps to conform to moving boundaries. The initial mesh used is unstructured and is generated using an in-house mesh generator based on the mixed Delaunay triangulation and the advancing front technique (see, for instance [71]). To reflect the complexity of the fluid domain, one may assign a suitable representative mesh size ($\mathrm{d}s$) on the free surface to the mesh generator, which indicates the characteristic distance between two connected nodes. For example, $\mathrm{d}s$ would be equal to approximately one-thirtieth of a wavelength. It should be noted that the specified mesh sizes may be different in the x-direction ($\mathrm{d}x$) and in the y-direction ($\mathrm{d}y$). In such a case, $\mathrm{d}s = \min(\mathrm{d}x, \mathrm{d}y)$. The mesh generator also needs a number of element layers (N_z) in the vertical direction, which is used to evaluate the vertical representative mesh size using an exponential function-based formulation suggested by Wu and Eatock Taylor [56]. Although $\mathrm{d}s$ and N_z are not precisely equal to the real mesh size and the real number of layers (actually the number of layers may be different at different positions), it largely indicates how fine the mesh is. It is noted that the QALE-FEM can also accept meshes from other mesh generators.

For moving the mesh at every time step, a novel methodology is suggested and adopted, in which interior nodes and boundary nodes are separately considered; and the nodes on the free surface and on rigid boundaries are treated differently. Nodes on the free surface are further split into two groups: those on waterlines and those not on waterlines (inner-free-surface nodes). Different methods are employed for moving different groups of nodes.

To move the interior nodes that do not lie on boundaries, a spring analogy method is used. In this method, nodes are considered to be connected by springs and the whole mesh is then deformed like a spring system. Specifically, the nodal displacement is determined by

$$\Delta \mathbf{r}_i = \sum_{j=1}^{N_i} k_{ij} \Delta \mathbf{r}_j \Bigg/ \sum_{j=1}^{N_i} k_{ij} \tag{5}$$

where $\Delta \mathbf{r}_i$ is the displacement of node I; k_{ij} is the spring stiffness and N_i is the number of nodes that are connected to node I. As pointed out by Ma and Yan [21], the spring analogy method was originally adopted to cope with aerodynamic problems without the free surface. To apply it to the problems associated with a large deformation of the free surface, the authors of this paper have considerably modified the method by proposing a robust and distinctive method for computing the spring stiffness:

$$k_{ij} = k_{ij}^0 \Psi^{fs} \Psi^{bs} \tag{6}$$

in which k_{ij} is the spring stiffness and k_{ij}^0 is given by

$$k_{ij}^0 = \frac{1}{l_{ij}^2} \tag{7}$$

DOI: 10.1002/fld

where l_{ij} is the distance between nodes i and j. Ψ^{fs} and Ψ^{bs} are the correction functions associated with the free surface and the moving rigid boundaries, respectively. Ψ^{bs} is taken as 1 in the cases without floating bodies [21]. Ψ^{fs} is defined as

$$\Psi^{fs} = \mathrm{e}^{\gamma_f[1+(z_i+z_j)/2d]} \tag{8}$$

where z_i and z_j are the vertical coordinates of nodes i and j; d is the water depth; and γ_f is a coefficient that should be assigned a larger value if the springs are required to be stiffer on the free surface. Numerical tests indicate that $\gamma_f = 1.7$ is suitable.

The positions of nodes on the free surface and waterlines are determined by physical boundary conditions, i.e. following the fluid particles at most time steps. The nodes moved in this way may become too close to or too far from each other. To prevent this from happening, these nodes are relocated at a certain frequency, e.g. once every 40 time steps. When doing so, the nodes on the waterlines are re-distributed by adopting a principle for a self-adaptive mesh, i.e. the weighted arc-segment lengths satisfy

$$\varpi_i \Delta s_i = C_s \tag{9}$$

where ϖ is a weight function and can be taken as 1, Δs_i the arc-segment length between two successive nodes and C_s a constant.

In order to relocate the inner-free-surface nodes, they are first moved using the spring analogy method in the projected plane of the free surface, resulting in new coordinates x and y; and then the elevations of the free surface corresponding to the new coordinates are evaluated by an interpolating method. In order to take into account of the local gradient of the free surface, however, the spring stiffness for moving the nodes in the x- and y-directions is determined, respectively, by:

$$k_{ij}^{(x)} = \frac{1}{l_{ij}^2}\sqrt{1+\left(\frac{\partial\zeta}{\partial x}\right)^2} \quad \text{and} \quad k_{ij}^{(y)} = \frac{1}{l_{ij}^2}\sqrt{1+\left(\frac{\partial\zeta}{\partial y}\right)^2} \tag{10}$$

where $k_{ij}^{(x)}$ and $k_{ij}^{(y)}$ are the spring stiffness for moving the free surface nodes in the x- and y-directions, respectively; $(\partial\zeta/\partial x)$ and $(\partial\zeta/\partial y)$ the local slopes of the free surface in the corresponding directions. It is noted that if a floating body is involved, Equation (10) should be changed to the one given by Ma and Yan [68].

3.2. Calculation of fluid velocity on the free surface

The mesh used in the QALE-FEM is arbitrarily unstructured and moves during the calculation. An effective method to calculate the fluid velocity on the free surface under this condition was developed in [21]. In this method, the velocity at a node I with neighbours J_k $(k=1,2,3,\ldots,m)$ on the free surface is split into normal and tangential components. The normal component $(\mathbf{v}_n)$ of the velocity is determined by a three-point finite difference scheme:

$$\mathbf{v}_n = \left[\frac{2}{3h_{I1}}\left(\frac{2h_{I1}+h_{I2}}{h_{I1}+h_{I2}}+\frac{1}{2}\right)\phi_I - \left(\frac{2}{3h_{I2}}+\frac{1}{h_{I1}}\right)\phi_{I1} + \frac{2}{3h_{I2}}\left(\frac{h_{I1}}{h_{I1}+h_{I2}}\right)\phi_{I2}\right]\mathbf{n} \tag{11}$$

where $\mathbf{n}$ is the unit normal vector of the free surface at the node, $I1$ and $I2$ represent the two points selected along the normal line; h_{I1} and h_{I2} are the distances between I and $I1$ and between $I1$ and $I2$, respectively; and ϕ_I, ϕ_{I1} and ϕ_{I2} denote the velocity potentials at the node and the two

DOI: 10.1002/fld

points; ϕ_{I1} and ϕ_{I2}, are found by a moving least-square method [25]. After the normal component of the velocity is determined, the tangential components of the velocity are calculated using a least-square method, in which each of the equations is given by

$$\mathbf{v}_{\tau_x}\cdot\mathbf{l}_{IJ_k}+\mathbf{v}_{\tau_y}\cdot\mathbf{l}_{IJ_k}=\mathbf{l}_{IJ_k}\cdot\nabla\phi-\mathbf{v}_n\cdot\mathbf{l}_{IJ_k}\quad(k=1,2,3,\ldots,m) \tag{12}$$

where $\mathbf{l}_{IJ_k}$ is the unit vector from node I to node J_k; $\mathbf{v}_{\tau_x}$ and $\mathbf{v}_{\tau_y}$ represent the velocity components in the $\boldsymbol{\tau}_x$ and $\boldsymbol{\tau}_y$ directions, respectively. $\boldsymbol{\tau}_x$ and $\boldsymbol{\tau}_y$ can be any two orthogonal unit vectors in the tangential plane of the free surface at node I. In this paper, they are determined by $\boldsymbol{\tau}_x=\mathbf{e}_y\times\mathbf{n}$ and $\boldsymbol{\tau}_y=\mathbf{n}\times\boldsymbol{\tau}_x$ if $|\mathbf{e}_y\times\mathbf{n}|\neq 0$; otherwise $\boldsymbol{\tau}_y=\mathbf{n}\times\mathbf{e}_x$, $\boldsymbol{\tau}_x=\boldsymbol{\tau}_y\times\mathbf{n}$, where $\mathbf{e}_x$ and $\mathbf{e}_y$ are the unit vectors in the x- and y-directions, respectively. Obviously, for 2D cases, this method is the same as that described by Ma and Yan [21].

4. NUMERICAL TECHNIQUE FOR MOVING MESH ASSOCIATED WITH 3D OVERTURNING WAVES

The new developments in this paper for dealing with problems concerning 3D overturning waves will be presented in the next two sections. They mainly contain the numerical techniques for moving the mesh and for computing the fluid velocity on the free surface when overturning occurs. The first one is presented in this section.

The basic strategy and principle to move the mesh are similar to that summarized above. Nevertheless, special consideration is devoted to the mesh near overturning jets when moving interior nodes and redistributing nodes on the free surface, which is discussed in the following two subsections.

For clarity, special nodes and elements are named before moving on. If a node is on the free surface and near or at the tip of an overturning jet, it is called Jet Node. One of them is shown in Figure 2 as a solid circle. In addition, if an element has one face on the free surface, the face is called outer face and the element is called free surface element.

4.1. Moving interior nodes

In the cases involving 3D overturning waves, the interior nodes are moved by the spring analogy method summarized above. Nevertheless, the interior nodes near jet nodes demand special care so as to result in elements of good quality. For this purpose, the stiffness of the springs in this area is assigned a relatively larger value. To do so, Ψ^{fs} in Equation (6) is changed to

$$\Psi^{fs}=\mathrm{e}^{\gamma_f\lfloor 1+(z_i+z_j)/2d\rfloor}(1+\gamma_{\mathrm{jet}}\delta_x\delta_y\delta_z) \tag{13}$$

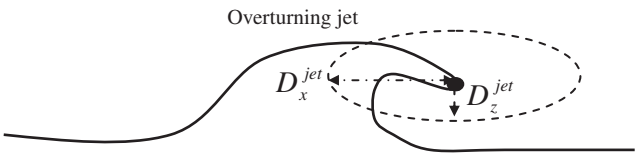

Figure 2. Illustration of an overturning jet and Jet Nodes.

DOI: 10.1002/fld

where γ_{jet} is a coefficient which is non-zero only if the free surface near the node concerned becomes vertical or overturning; δ_x, δ_y and δ_z are correction functions in the x-, y- and z-direction, respectively. They are all in a similar form and one of them is given by

$$\delta_x = \begin{cases} 1 - d_x / D_x^{\text{jet}} & d_x < D_x^{\text{jet}} \\ 0 & d_x \geqslant D_x^{\text{jet}} \end{cases} \tag{14}$$

in which subscript x can be replaced by y or z to give δ_y and δ_z. d_x (d_y or d_z) is the distance between the centre of Spring i-j and the nearest jet node in the x- (y- or z-) direction; D_x^{jet}, D_y^{jet} and D_z^{jet} indicate the maximum distance in different directions (Figure 2). According to the numerical tests so far, $\gamma_{\text{jet}} = 0.5$, $D_x^{\text{jet}} = D_y^{\text{jet}} = 10\,\text{d}s$ and $D_z^{\text{jet}} = 0.5H$ are appropriate, where H is the wave height.

Obviously, the above method works only if all the Jet Nodes are known. For 3D overturning waves, there may be many Jet Nodes. To find them, the following parameter is calculated for each free surface node, e.g. Node i:

$$c_{\min,i} = \min(\mathbf{n}_J \cdot \mathbf{n}_K), \quad J, K = 1, 2, 3, \ldots, NE_{sf,i}, \quad J \neq K \tag{15}$$

where subscripts J and K denote the element numbers, $NE_{sf,i}$ are the total number of all the free surface elements connected to node i, $\mathbf{n}_J$ is the outward unit normal vectors of the outer face of a element. In this paper, if $c_{\min,i} < 0.5$, Node i is considered as a Jet Node.

Furthermore, when a wave is overturning, the free surface near the overturning jet may have an extremely large deformation (Figure 2) which makes the elements easier to distort than in the earlier applications [21, 67, 69, 70]. In order to preserve the element shape during the mesh moving procedure, the ability of resisting torsion of elements needs to be enhanced in such an area. To do so, one may attach torsional springs to the vertexes of every element (referred as the torsional spring analogy method [72]) or introduce additional linear springs that resist the motion of an element vertex towards its opposite face (referred as the ball-vertex spring analogy method [73]). However, the force transformation and displacement conversion in the torsional spring analogy method and the additional springs in the ball-vertex spring analogy method consume extra computational resources and therefore reduce the efficiency. Alternatively, this aim can also be achieved by modifying the linear spring stiffness, considering the angular or volume changes of the elements, which needs less computational cost. For example, Zeng and Ethier [74] developed a 3D semi-torsional spring analogy method where the facing angle of each spring is taken into account when calculating the spring stiffness. This idea is extended here by introducing coefficients related to the quality of elements, i.e. the k_{ij}^0 in Equation (7) and Ψ^{bs} in Equation (6) are replaced by

$$k_{ij}^0 = \frac{1}{l_{ij}^2} + \alpha \sum_{m=1}^{NE_{ij}} \frac{1}{\sin^2 \theta_m^{ij}} \tag{16}$$

$$\Psi^{bs} = 1 / q_{\min}^{ij} \tag{17}$$

where NE_{ij} is the total number of elements sharing spring $i-j$, θ_m^{ij} is the angle between two faces of the mth element as shown in Figure 3, α is an coefficient. $q_{\min}^{ij}$ is the minimum value of the

DOI: 10.1002/fld

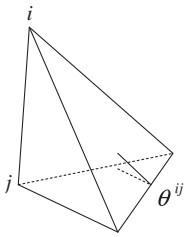

Figure 3. Facing angle in a tetrahedron element.

quality indexes of all the elements sharing spring $i-j$. The quality index for a single element e is defined as

$$q_e = \frac{3R_{\mathrm{i}}^e}{R_{\mathrm{c}}^e} \tag{18}$$

where R_{i} and R_{c} are the inradius and circumradius of the element, respectively. This quality index is based on the fact that the best tetrahedron element is the regular tetrahedron whose circumradius is three times of the inradius (see, for example [25, 75]). The range of its value is from 0 to 1. It equals to 1 for a regular tetrahedron and 0 for an element whose 4 nodes are located in one plane. A similar correction to Equation (17) was also made for problems associated with floating bodies by Ma and Yan [68].

According to our numerical investigations [25], the coefficient α is chosen by

$$\alpha = \begin{cases} 0, & q_{\min} > q_0 \\ 1, & q_{\min} \leqslant q_0 \end{cases} \tag{19}$$

where q_0 is a control parameter equal to 0.02; $q_{\min}$ is the minimum value of the quality indexes of all elements in the whole computational domain. It can be seen from Equations (16) and (19) that when the worst element has a quality index less than 0.02, the term

$$\sum_{m=1}^{NE_{ij}} \frac{1}{\sin^2 \theta_m^{ij}}$$

becomes effective. In addition, dividing $q_{\min}^{ij}$ in Equation (17) renders springs stronger when the quality index is reduced. All these help enhance the quality of elements.

4.2. Redistributing inner free surface nodes

As discussed by Yan and Ma [68, 69], the method to redistribute free-surface nodes outlined in Section 3.1 can only deal with problems where the free surface can be expressed as a single-valued function of x and y, e.g. in cases without overturning waves. The authors of this paper have developed an approach to redistribute nodes on a multi-valued body surface [68]. The same idea will be used here to redistribute the inner free surface nodes when overturning occurs. This approach is based on a local coordinate system formed by the local tangential lines and normal line at the node concerned. In this local coordinate system, the surface is always single valued, i.e. there is only one intersecting point between the free surface and a line parallel to the local normal

DOI: 10.1002/fld

line (and, of course, perpendicular to the local tangential lines). A node, e.g. i, is first moved in the tangential plane formed by tangential lines by

$$\Delta \mathbf{r}_{i\tau_i} = \sum_{j=1}^{N_i} k_{ij} \Delta \mathbf{r}_{j\tau_i} \Big/ \sum_{j=1}^{N_i} k_{ij} \tag{20}$$

where $\Delta \mathbf{r}_{i\tau_i}$ represents the displacement of node i in the tangential plane. After that, a new position of the nodes on the free surface is found by interpolation in the local coordinate system. In order to consider the effect of the overturning jet, the spring stiffness for moving inner-free-surface nodes is assigned as

$$k_{ij} = \frac{1}{l_{ij}^2}(1 + \gamma_{\text{jet}} \delta_x \delta_y \delta_z) \tag{21}$$

where γ_{jet}, δ_x, δ_y and δ_z are the same as those in Equation (13). It is noted that the effect of the local gradient of the free surface involved in Equation (10) is implicitly taken into account here because of the use of the local coordinate system.

5. NUMERICAL TECHNIQUE FOR CALCULATING FLUID VELOCITY NEAR OVERTURNING JETS

The principle for calculating the fluid velocity on the free surface is similar to that summarized in Section 3.2, in which the fluid velocity is split into the normal and the tangential components and different schemes are used to calculate different velocity components. The accuracy of the normal velocity component in Equation (11) depends on the estimation of ϕ_{I1} and ϕ_{I2}, for which a moving least-square method is used. For a node near the overturning jet, interior nodes around Points $I1$ and $I2$ may be only few and unevenly distributed about the normal line, as shown in Figure 4(a). This degrades the accuracy of the velocity calculation. In order to tackle the problem, a special treatment is applied in such a situation, which is similar to that for the nodes near the rigid boundary suggested by Ma and Yan [21]. That is, Equations (11) and (12) are still used, but the normal vector $\mathbf{n}$ is replaced by another unit vector $\mathbf{n}_r$ (Figure 4(b)). Accordingly, instead of tangential vectors $\boldsymbol{\tau}_x$ and $\boldsymbol{\tau}_y$, two other vectors ($\boldsymbol{\tau}_{rx}$ and $\boldsymbol{\tau}_{ry}$) perpendicular to $\mathbf{n}_r$ are employed.

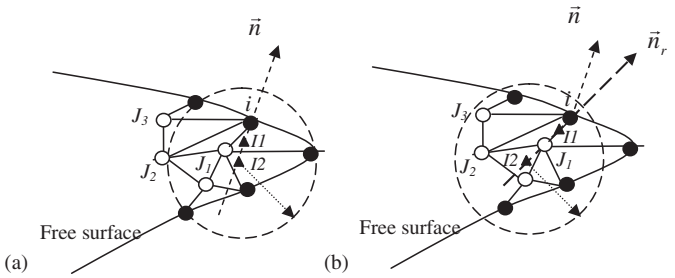

Figure 4. Elements near the overturning jet (solid circle: free surface nodes; hollow circle: interior nodes; solid triangles: point $I1$ or $I2$; dashed circle: influence domain of $I2$ for estimating the velocity potential at this point).

DOI: 10.1002/fld

To describe how to define $\mathbf{n}_r$, take node i as an example (Figure 4(b)). It lies on the free surface and the interior nodes $J_1, J_2, J_3, \ldots, J_M$ are connected with it. The angle α_{iK} between $\mathbf{n}$ and each vector of $\mathbf{x}_i - \mathbf{x}_{J_k}$ $(K = 1, 2, \ldots, M)$ is estimated by

$$\cos\alpha_{iK} = \mathbf{n} \cdot (\mathbf{x}_i - \mathbf{x}_{J_k}) / |(\mathbf{x}_i - \mathbf{x}_{J_k})| \tag{22a}$$

If $J_{K\min}$ is the interior node whose angle is $\alpha_{iK\min} = \min\{\alpha_{i1}, \alpha_{i2}, \ldots, \alpha_{iM}\}$, $\mathbf{n}_r$ is then chosen to pass the node and estimated by

$$\mathbf{n}_r = (\mathbf{x}_i - \mathbf{x}_{J_{K\min}}) / |\mathbf{x}_i - \mathbf{x}_{J_{K\min}}| \tag{22b}$$

After determining $\mathbf{n}_r$, $\boldsymbol{\tau}_{rx}$ and $\boldsymbol{\tau}_{ry}$ are given in the similar way as for $\boldsymbol{\tau}_x$ and $\boldsymbol{\tau}_y$ in Equation (12), i.e. $\boldsymbol{\tau}_{rx} = \mathbf{e}_y \times \mathbf{n}_r$ and $\boldsymbol{\tau}_{ry} = \mathbf{n}_r \times \boldsymbol{\tau}_{rx}$ if $|\mathbf{e}_y \times \mathbf{n}_y| \neq 0$; otherwise $\boldsymbol{\tau}_{ry} = \mathbf{n}_r \times \mathbf{e}_x$, $\boldsymbol{\tau}_{rx} = \boldsymbol{\tau}_{ry} \times \mathbf{n}_r$. To determine the two points along the new vector $\mathbf{n}_r$, the values of h_{I1} and h_{I2} in Equation (11) are assigned to be 0.6 times the distance between node i and node $J_{K\min}$. It can be understood that after applying the special treatment, the two points $I1$ and $I2$ should have more interior nodes in their influence domain for estimating the velocity potential at this point, more evenly distributing about the line $\mathbf{n}_r$, than those in Figure 4(a) and therefore the accuracy of the velocity is improved.

6. VALIDATION AND CONVENGENCE INVESTIGATION

In this section, the QALE-FEM is validated by comparing its numerical predictions with published results obtained by using other numerical methods or experiments. Owing to the fact that almost all the experiments regarding overturning waves are two dimensional, some 2D cases will be considered together with 3D cases. For a 2D case, the width of the tank is taken as $2d$ and all parameters do not vary along the y-direction, making it a y-independent 3D problem in order to use the 3D QALE-FEM. Effort is also devoted to the investigations on the convergent properties of this method. For all the cases presented below, the parameters with a length scale are nondimensionalized by the water depth d and other parameters by g and d, such as

$$t \to \tau\sqrt{d/g} \quad \text{and} \quad \omega \to \omega\sqrt{g/d}$$

where τ is the nondimensionalized form of the time.

6.1. Selection of time steps

In order to achieve convergent results, the time step must be properly selected. It can be understood that the required time step $(\Delta\tau)$ is a function of the characteristic minimum mesh size $(\mathrm{d}s_{\min})$ and the characteristic particle velocity (U_c). It may be determined by

$$\Delta\tau = c_t \frac{\mathrm{d}s_{\min}}{U_c} \tag{23}$$

which is similar to the well-known Courant condition, where c_t is a coefficient less than 1. In the correction function for spring stiffness in Equation (13), the maximum value of the term $1 + \gamma_{\text{jet}}\delta_x\delta_y\delta_z$ is $1 + \gamma_{\text{jet}}$, occurring near the overturning jets, and its minimum value is 1, occurring in other areas away from the overturning jets. In addition, $\mathrm{d}s_{\min}$ should occur near the overturning jets. Therefore, it may stand to reason that $\mathrm{d}s_{\min}$ should be related to the representative mesh size $(\mathrm{d}s)$ and can be estimated by $\mathrm{d}s_{\min} = \mathrm{d}s/(1 + \gamma_{\text{jet}})$.

DOI: 10.1002/fld

For periodic waves, ds can be correlated to λ/N_m, where λ is the characteristic wavelength estimated by $\lambda=(2\pi/k)$ and $\omega^2=k\tanh(k)$ for a specified wave frequency ω, and N_m is the averaged number of elements in one wavelength. In such a situation, U_c may be chosen as $U_c=\lambda/T$ (the celerity of a linear wave) and thus Equation (23) becomes

$$\Delta\tau=\frac{c_t}{1+\gamma_{\text{jet}}}\frac{T}{N_m} \tag{24}$$

For solitary waves that do not have a finite wavelength, one may use $U_c=1$ and obtain

$$\Delta\tau=\frac{c_t\,\mathrm{d}s}{1+\gamma_{\text{jet}}} \tag{25}$$

The last equation is similar to that in [28, 41] for determining the time step when simulating solitary waves by using the BEM.

According to our numerical investigations [25] for regular water waves without overturning, where $\gamma_{\text{jet}}=0$, the maximum time step for the QALE-FEM to achieve acceptable results is $T/64$ for strongly nonlinear waves (wave steepness up to 0.1) and $T/32$ for linear waves if the initial mesh size is about $\lambda/30$. Based on this and Equation (24), c_t is not necessarily less than 0.45 for waves without overturning. However, the value of c_t may not be suitable for the cases with overturning.

To test what value of c_t is suitable for the QALE-FEM to model overturning waves, the case studied by Grilli *et al*. [41] is considered here, which was also used to validate simulation of 3D overturning waves by Grilli *et al*. [28]. In this case, the length and width of the tank are 18 and 2, respectively. A seabed with the slope of 1:15 in the x-direction starts from $x_0=5.4$ and truncated at $x_t=18$. As in the above two references, the solitary wave is initialized by using Tanaka's method [76] which gives 'exact' solution for the wave profile, the velocity potential and the fluid velocity on the free surface. The initial wave height (H) is 0.6 and the initial crest is located at $x=5.5$. ds is selected as 0.05 in both the x- and y-directions and $N_z=12$. The numerical results by the QALE-FEM are first compared with those obtained by Grilli *et al*. [28] to ensure the computation to be sufficiently accurate. In this comparison, c_t is taken as 0.45 (time step is 0.015). The free surface profiles at two different instants are plotted in Figure 5. Curve (a) corresponds to the state that the tangential direction of the front face of the crest tends to become vertical. Curve (b) shows the results after the overturning wave occurs. At both instants, the QALE-FEM leads to almost the same results as the BEM model.

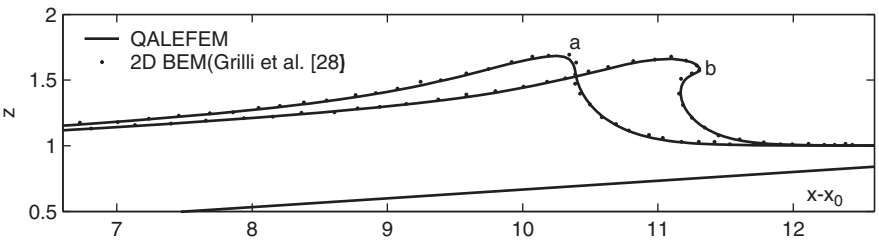

Figure 5. Comparison of the wave profiles from the QALE-FEM and the BEM for 2D solitary wave at different instants (a: $\tau\approx7.55$; b: $\tau\approx8.16$; $H=0.6$; slope: $\frac{1}{15}$).

DOI: 10.1002/fld

The cases with different values of c_t are then considered. For this purpose, they are chosen as 0.375, 0.45, 0.5 and 0.6, respectively. The wave profiles at $\tau \approx 8.16$ obtained by using these values of c_t are plotted in Figure 6. It is found that the differences between all the cases shown in this figure are negligible. However, the computation with $c_t = 0.6$ quickly ceases after this instant. This indicates that c_t should not be larger than 0.5 and not necessarily less than 0.375 for simulating overturning waves in this case by using the QALE-FEM. This range of the c_t value for the present method is not much different from (0.45–0.5) that suggested by Grilli *et al.* [28] for the BEM.

6.2. Numerical validation

In this subsection, the method will be validated by using both 2D and 3D solitary waves in different configurations. 2D cases are first considered, for which experimental results are available.

6.2.1. Overturning of 2D solitary waves over seabeds with different geometries. A preliminary comparison with 2D results of Grilli *et al.* [28] has been presented in the above subsection to investigate the proper value of c_t, which showed a good agreement. Two other cases are presented here to further show the accuracy of the QALE-FEM.

In the first case, a 2D solitary wave propagating over a submerged step is considered. The configuration is sketched in Figure 7, in which P2, P3 and P4 are wave gauges. The similar set-up has been used by Yasuda *et al.* [24] in their experiment, whose results have been used by many researchers for the purpose of validation (e.g. Helluy *et al.* [26] and Devrard *et al.* [27]). In our study, the parameters are the same as in Devrard, *et al.* [27] but they are here nondimensionalized by the water depth, which is 0.31 m in that reference. The left side of the tank is located at $x = 0$.

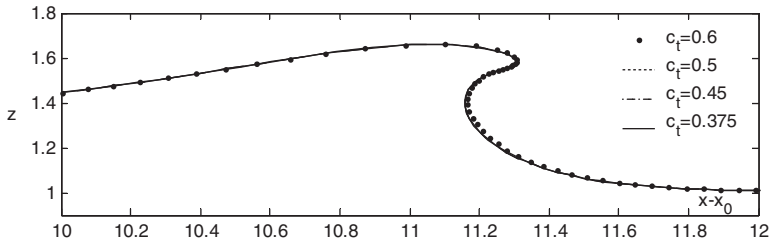

Figure 6. Free surface profiles at $\tau \approx 8.16$ obtained by using different time steps ($H = 0.6$; slope: $\frac{1}{15}$).

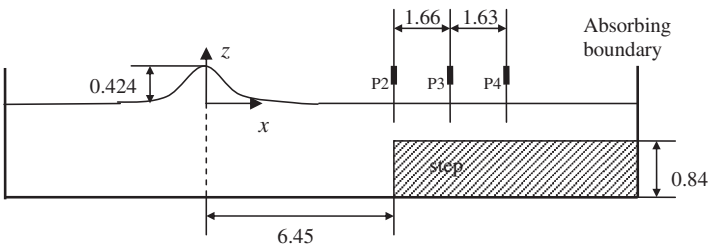

Figure 7. Sketch of the configuration for the case with a submerged step.

DOI: 10.1002/fld

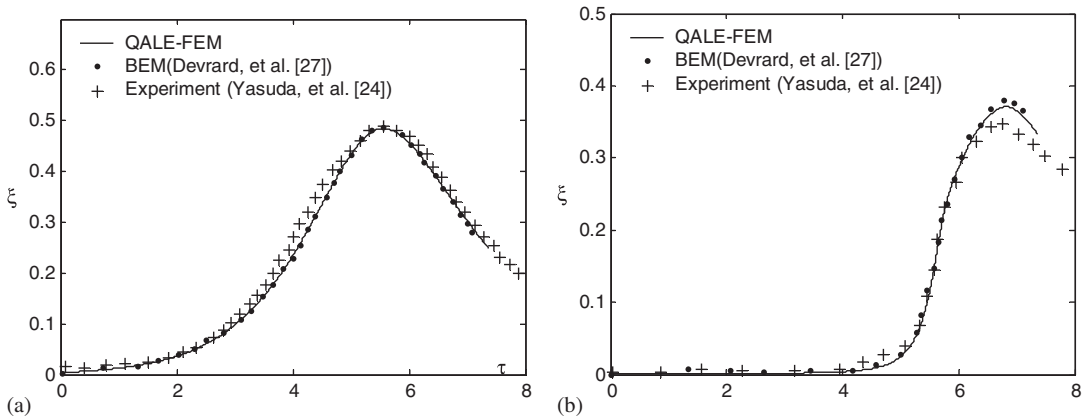

Figure 8. Wave elevation recorded by different gauges ($H=0.424$; step height: 0.848): (a) gauge P2 and (b) gauge P3.

The submerged step with a height of 0.848 starts from $x_0=12.9$. The solitary wave is generated by specifying the initial position of and the velocity potential on the free surface given by using Tanaka's method [76] with the initial crest located at $x=6.45$ and the wave height (H) being 0.424. An absorbing boundary condition is applied at the right side of the tank. ds is taken as 0.05 on the free surface and N_z is specified as 12. c_t in this case is taken as 0.5. Figure 8 shows the wave histories recorded at wave gauges P2 and P3. For the purpose of comparison, the experimental data from Yasuda *et al.* [24] and the numerical results from the BEM by Devrard *et al.* [27] are plotted together. From this figure, it is observed that the results from the QALE-FEM agree well with those from the BEM method, and that both numerical results are very close to the experimental data.

In the second case, the solitary wave is generated by a flap paddle wavemaker with the motion angle and angular velocities specified. The same case in the experiment by Kimmoun *et al*. [77] is used as described by Grilli *et al.* [43]. In our computation, the wavemaker motion parameters are taken from Grilli *et al.* [43]. By using these parameters, the height of the generated solitary wave is about $H=0.135$. In this case, the numerical tank has the length of 18 and the width of 2. A composite sloping seabed starts from $x_0=6.45$. The slope of the seabed are $\frac{1}{6}$ from $x=x_0$ to $x=x_0+2$ but becomes $\frac{1}{15}$ when $x>x_0+2$. ds is 0.04 and the time step is determined again by using $c_t=0.5$. Figure 9 shows the comparison of free surface profiles near the overturning jet calculated by the QALE-FEM with the experimental data from Kimmoun *et al*. [77] and the numerical results by the BEM from Grilli *et al.* [43]. A similar agreement with numerical results by the BEM and the experimental data to the case shown in Figure 8 is observed from this figure.

6.2.2. Overturning of a solitary wave over a 3D symmetrical seabed. Experiments on 3D overturning solitary waves have not been found. The numerical results from Grilli *et al*. [28] for solitary waves propagating over a 3D sloping ridge are used here to validate our method. The 3D ridge is expressed as

$$z=s_c(x-x_0)\,\mathrm{sech}^2(k_c y) \tag{26}$$

DOI: 10.1002/fld

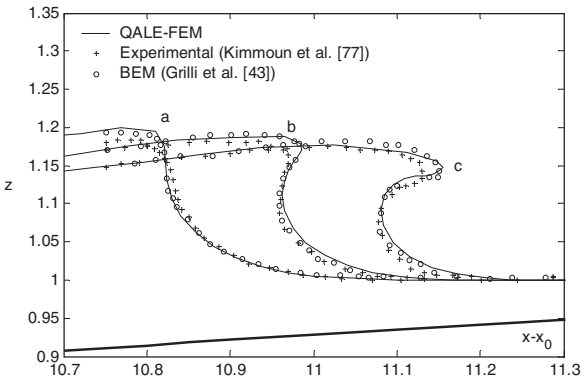

Figure 9. Free surface profiles recorded at different time steps ($H=0.135$).

where x_0 is the location where the sloping seabed starts, s_c is the slope at $y=0$ and $\mathrm{sech}^2(k_c y)$ is the transverse modulation of the slope along the y-direction depending on the coefficient k_c which is constant with respect to y in [28]. That means that the seabed geometry in those applications is symmetrical about $y=0$. In this case, the length and the width of the tank are 19 and 8, respectively. The ridge starts from $x_0=5.225$. s_c is $\frac{1}{15}$ and k_c is taken as 0.25. The solitary wave is generated by using the same method as for Figure 8. The wave height is 0.6 with the initial crest located at $x=5.7$. ds is specified as 0.07 for generating the mesh and the value of c_t is 0.5 for determining the time step.

Figures 10 and 11 show the free surface profiles on the side walls ($y=\pm 4$) and in the central plane ($y=0$) of the tank at different instants. For this case, Grilli *et al*. [28] gave the results up to $\tau\approx 8.57$ and presented the corresponding free surface profiles at $\tau=8.25$ and 8.57. Guyenne and Grilli [51] used a finer grid and obtained results up to $\tau=9.14$. We took the results at $\tau=8.25$ and 8.57 from Grilli *et al*. [28] and those at $\tau=7.89$ and 8.827 from Guyenne and Grilli [51] for the comparison. Obviously, the results shown in Figure 10, well before overturning, are almost the same as those from the papers using the BEM. For the free surface profiles at $y=0$ in Figure 11, the Curves (c) and (d) show slight differences near the overturning jet. In order to analyse the accuracy, the relative errors in mass (ε_m) and energy (ε_e) are estimated by using the same method as in Grilli *et al*. [28]. The relative errors in mass at these two time steps are 0.09% and 0.2%, respectively, and the corresponding relative errors in energy are 0.16% and 0.43%, respectively. All the errors can be considered as very small.

6.3. Convergence tests on initial representative mesh sizes

In the cases shown above, the solitary waves with different heights and over different seabeds are modelled by using specified mesh sizes. As discussed in our previous papers [68, 69], the main factors that affect the convergence property of the QALE-FEM are the time step and the mesh size for the cases without floating bodies. In Section 6.1, the effect of the time steps on the results has been investigated. In this section, discussions are devoted to the effect of the representative mesh size (ds) to ensure the numerical results given are convergent. Although convergence investigations have been made for all the cases shown in this paper, only the analysis for the 3D case shown in Figure 11 is presented in this section. For this purpose, the values of ds are selected to be 0.05, 0.07, 0.085 and 0.1. All other parameters remain the same as for Figure 11.

DOI: 10.1002/fld

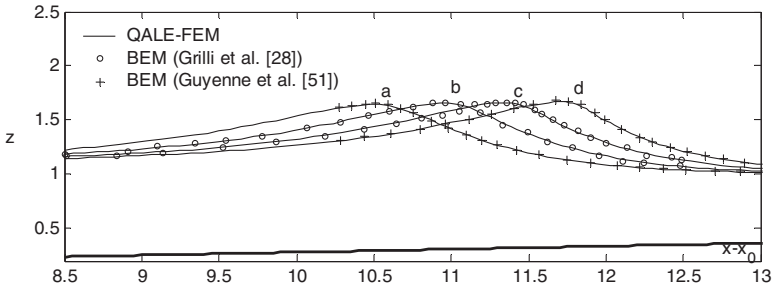

Figure 10. Free surface profile at $y=\pm 4$ ($H=0.6$; $s_c=\frac{1}{15}$; $k_c=0.25$; d$s=0.07$; Curve a: $\tau\approx 7.89$; b: $\tau\approx 8.25$; c: $\tau\approx 8.57$; d: $\tau\approx 8.827$; thick solid line represents the seabed geometry).

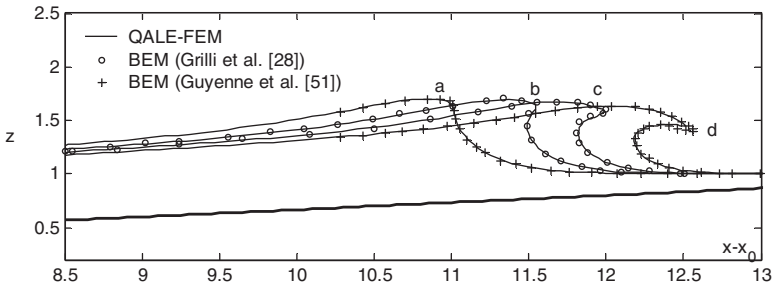

Figure 11. Free surface profile at $y=0$ ($H=0.6$; $s_c=\frac{1}{15}$; $k_c=0.25$; d$s=0.07$; Curve a: $\tau\approx 7.89$; b: $\tau\approx 8.25$; c: $\tau\approx 8.57$; d: $\tau\approx 8.827$; thick solid line represents the seabed geometry).

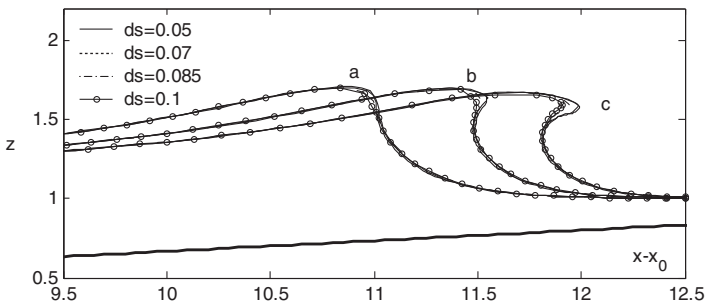

Figure 12. Free surface profile at $y=0$ in different instants ($H=0.6$; $s_c=\frac{1}{15}$; $k_c=0.25$; a: $\tau\approx 7.89$; b: $\tau\approx 8.25$; c: $\tau\approx 8.57$).

Figure 12 shows the free surface profile at $y=0$. The results for all the cases corresponding to different values of ds agree well with each other, though there is visible difference near the overturning jet in Curves (b) and (c) between the results of d$s=0.1$ and others. Even using the coarsest mesh (d$s=0.1$), the relative errors in the mass and energy at $\tau\approx 8.57$ are about 0.11% and 1.21%, respectively. Therefore, d$s=0.1$ is acceptable for the purpose of predicting

DOI: 10.1002/fld

the occurrence of the overturning before forming a jet. However, for studying the properties of overturning with a jet, finer meshes ($ds \leqslant 0.085$) are preferred for this case.

The investigation in this subsection demonstrates that the representative mesh sizes selected in the previous subsection are appropriate. However, it is noted that the appropriate mesh size is problem dependent and it must be carefully selected for different cases as in all other numerical methods.

6.4. Computational efficiency

All comparisons of the numerical results obtained by the present method with the experimental data and the results by other methods may lead to one conclusion, i.e. the QALE-FEM can simulate overturning waves at the same level of accuracy as the BEM method based on the same FNPT model. One may ask how about its efficiency. In this subsection, attention is concentrated on discussions about the computational efficiency of the QALE-FEM. Ma and Yan [21] pointed out that the QALE-FEM might use only 15% of the CPU time required by the conventional FEM. Its efficiency is now compared with the BEM using the case shown in Figure 11.

As mentioned before, Grilli *et al*. [28] developed a high-order BEM model that is believed to be the most efficient model for overturning waves at that time. To obtain the results up to $\tau \approx 8.57$ for the case in Figure 11, they used a coarser quadrilateral grid ($50 \times 20 \times 4$) for the first 70 time steps and then used a finer grid ($60 \times 30 \times 4$) for the next 120 time steps. The total CPU time spent on the two stages is about 52.8 h on a supercomputer (CRAY-C90). Fochesato and Dias [54] developed a fast BEM method, which may be 6 times faster than the conventional BEM [28] as pointed out by the authors. Their calculations for the same case were also split into two stages. They used a coarser grid ($40 \times 10 \times 4$) with 1422 boundary nodes for the first stage ($\tau < 6$, about 54 time steps) and then a finer grid ($60 \times 40 \times 4$) with 6022 boundary nodes for the rest of calculation (200 time steps). Totally, they spent about 19 h to achieve the results up to $\tau \approx 8.57$ by using a PC (2.2 GHz processor, 1G RAM). Our simulations of the same case are run on a PC with 2.53 GHz processor and 1 G RAM. The computer is largely similar to that used by Fochesato and Dias [54], though the processor is slightly faster. The CPU time taken by the QALE-FEM for simulation up to $\tau \approx 8.57$ and the relative error in the cases with different representative mesh sizes are displayed in Table I. In some of these cases, the representative mesh size is different in the x- and y-directions, i.e. $dx \neq dy$, to show more variations. As could be seen from the table, the QALE-FEM takes only 0.91 h (or 54 min) to produce the results with acceptable errors in mass and energy ($\varepsilon_m = 0.1\%$ and $\varepsilon_e = 0.26\%$, respectively). Even to achieve higher accuracy of $\varepsilon_m = 0.09\%$ and $\varepsilon_e = 0.16\%$, which are smaller than those errors given by Fochesato and Dias [54], the CPU time taken by the

Table I. Computational efficiency of the QALE-FEM for the case shown in Figure 11.

dx	dy	N_t	N_b	$\Delta\tau$	CPU/step (s)	Total (h)	ε_m (%)	ε_e (%)
0.100	0.100	139 239	38 106	0.03333	9.0	0.65	0.11	1.21
0.085	0.100	164 025	44 550	0.02833	10.2	0.91	0.10	0.26
0.085	0.085	235 125	52 650	0.02833	14.5	1.22	0.10	0.26
0.070	0.100	230 384	53 856	0.02333	14.0	1.41	0.09	0.17
0.070	0.070	314 160	69 088	0.02333	18.0	1.80	0.09	0.16
0.050	0.050	448 437	98 334	0.01667	26.6	3.81	0.03	0.09

DOI: 10.1002/fld

QALE-FEM is only 1.8 h (or 108 min). Therefore, for this particular case, the QALE-FEM can be at least 10 times faster than the fast BEM method.

6.5. *Application*: *3D overturning waves over complex seabeds*

So far, all 3D results presented are symmetrical about the $y=0$ plane. It is understandable that the overturning properties, such as when and where the overturning occurs, will be different if the seabed is non-symmetrical about the $y=0$ plane. To see how different the properties are and to show the flexibility of the QALE-FEM, the method is employed to model solitary waves over a non-symmetrical seabed about $y=0$. In this investigation, the length and the width of the tank are the same as those in Figure 11. The seabed geometry is also expressed by Equation (26) with the same x_0 and s_c, which are 5.225 and $\frac{1}{15}$, respectively, but with different variation of k_c. In this case, the k_c for $y>0$ (referred as k_c^+) is 0.25, the same as Figure 11; however, that for $y<0$ (referred as k_c^-) is 1.0. The representative mesh size is taken $ds=0.07$.

Figure 13 shows the free surface profiles recorded at $\tau\approx 8.57$, the same instant as shown by Curve *c* in Figure 12, for cases with different k_c^-. One can see from this figure, that at this instant, the overturning jet in the case with $k_c^-=1.0$ (Figure 13(b)) is not evident. However, that in the case with $k_c^+=k_c^-=0.25$ (Figure 13(a)), the same case as shown in Figure 11, seems to be well developed. This implies that the breaking time varies as the change of seabed geometry. To further show how the overturning jet develops in the case with non-symmetrical seabed, the free surface profiles at two other instants after overturning starts are plotted in Figure 14.

As can be seen, the free surface profiles in Figure 14 are non-symmetrical about $y=0$, as expected. It is also observed that the overturning does not start to occur at $y=0$; instead, it occurs in the area $y>0$. This is quite different from the above symmetrical cases in which the overturning

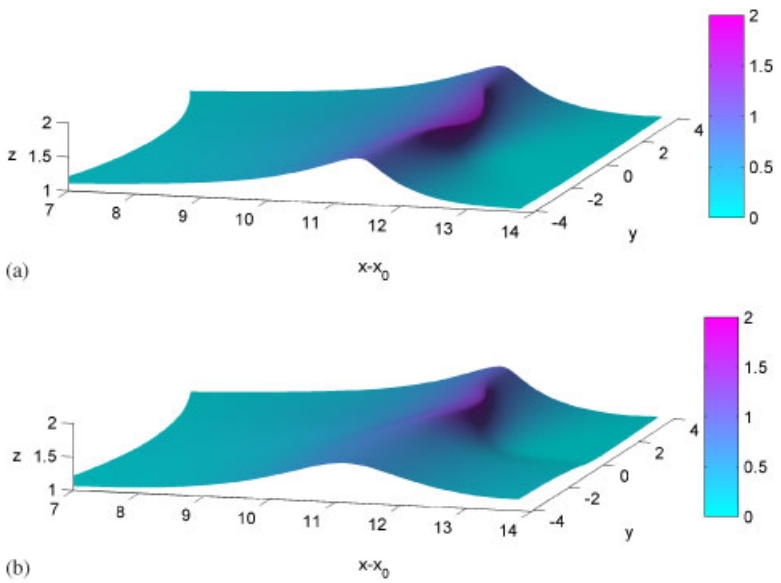

Figure 13. Free surface profiles at $\tau\approx 8.57$ in the cases with different k_c^- ($H=0.6$; $s_c=\frac{1}{15}$; $k_c^+=0.25$; the colour bar represents the speed ($|\nabla\phi|$) on the free surface): (a) $k_c^-=0.25$ and (b) $k_c^-=1.0$.

DOI: 10.1002/fld

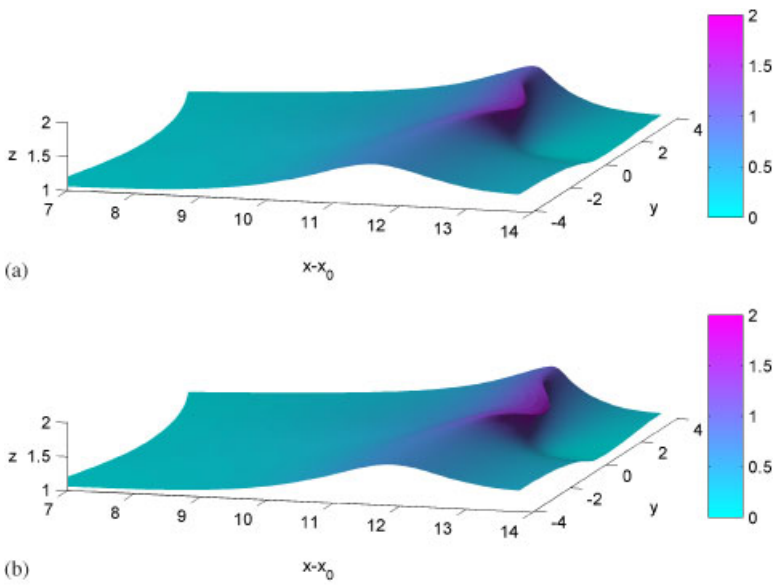

Figure 14. Free surface profiles at different instants after overturning over non-symmetrical seabed ($H=0.6$; $s_c=\frac{1}{15}$; $k_c^+=0.25$ and $k_c^-=1.0$; the colour bar represents the speed ($|\nabla\phi|$) on the free surface): (a) $\tau\approx 8.95$ and (b) $\tau\approx 9.16$.

always starts to occur at $y=0$. This is clearer in Figure 15 that shows the free surface profiles at several longitudinal vertical planes with different y-coordinates.

Figure 15(a) evidently shows that the wave front at $y=0.8$ reaches the farthest position in the x-direction at $\tau\approx 8.55$ while those at the other two longitudinal planes, i.e. at $y=0.5$ and 1.1 (which are symmetrical about the plane at $y=0.8$) are behind it and both are very close to each other. All of them are considerably farther than the wave front at $y=0$. Figure 15(b) gives the results when the overturning just occurs at $y=0$ while the overturning jet has been well developed at other three vertical planes. It is interesting to point out that the wave front at $y=1.1$ now clearly departures from the front at $y=0.5$ and becomes closer to the front at $y=0.8$ and also that the jet at $y=1.1$ is as sharp as the jet at $y=0.8$ but much sharper than the jet at $y=0.5$. This observation is confirmed by curves in Figure 15(c). All these facts indicate that the overturning jet is moving gradually towards the wall of $y=4$. This seems to suggest that the overturning jets may be guided to occur in some areas by changing the seabed geometry in order to prevent them from happening at places where important structures sit near the shore.

More cases with different incident waves and different seabed geometries have also been simulated, such as solitary waves propagating over non-symmetrical seabeds with different combinations of k_c^- and k_c^+, transient oscillating waves overturning over bumps or artificial reefs on a slope. We could not present all the results in one paper but more illustrations will be given in the rest of this subsection. For this purpose, some snapshots of overturning waves are shown in Figures 16 and 17. Figure 16 displays the wave profiles with well-developed overturning jets for the case with $k_c^+=0.25$ and $k_c^-=0.1$. All other parameters for this figure are the same as for Figure 15, except for k_c^- that is now less than k_c^+. It can be seen that the overturning now takes

DOI: 10.1002/fld

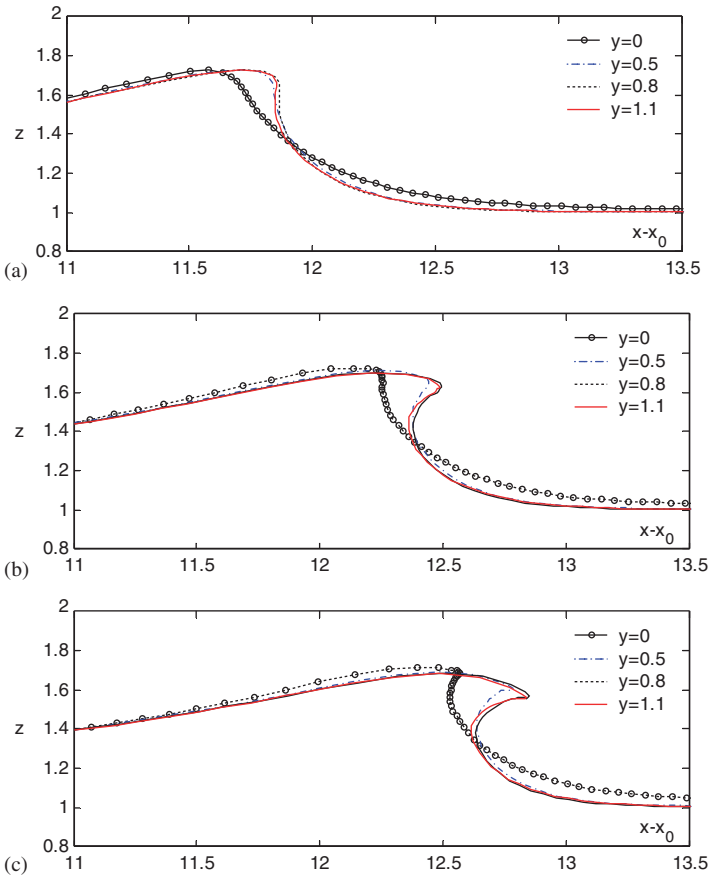

Figure 15. Free surface profiles at different longitudinal planes ($H=0.6$; $s_c=\frac{1}{15}$; $k_c^+=0.25$ and $k_c^-=1.0$; x_0 is the initial position of the crest of the solitary wave): (a) $\tau\approx 8.55$; (b) $\tau\approx 8.95$; and (c) $\tau\approx 9.16$.

place in the area of $y<0$, rather than $y>0$ in Figure 14. This confirms that wave overturning can be guided to avoid some area by changing seabed geometry. Figure 17 illustrates the free surface profile for a transient oscillating wave overturning over several artificial reefs on a slope, which is generated by a piston wavemaker subjected to a harmonic motion. In this case, two groups of overturning jets are observed at the same time. Each group embodies three jets and the jets are different from each other. This figure also reveals some interesting points, i.e. overturning does not only occur above the reefs but also beyond them and several different overturning jets may simultaneously take place.

7. CONCLUSION

In this paper, the QALE-FEM has been further developed to model 3D overturning waves. In this method, the boundary value problem for the velocity potential is solved by using a finite

DOI: 10.1002/fld

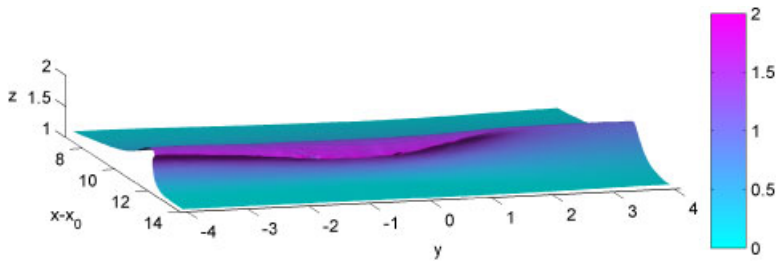

Figure 16. Free surface profiles at $\tau \approx 8.70$ for $k_c^+ = 0.25$ and $k_c^- = 0.1$, ($H = 0.6$; $s_c = \frac{1}{15}$, the colour bar represents the speed ($|\nabla\phi|$) on the free surface).

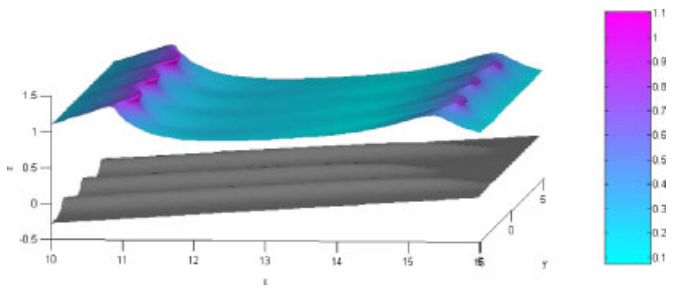

Figure 17. Free surface profiles in cases with three artificial reefs for $\tau \approx 26.68$. The three reefs are centred at ($x_c = 11, y_c = 0$), ($x_c = 11.5, y_c = 3$) and ($x_c = 12, y_c = -3$), respectively. Each reef is defined by $z = 0.2(1 - e^{-1.7(|x-x_c|+4)}) \sec h^2[2(y - y_c)]$. The amplitude (a) and frequency (ω) of the wavemaker to generate the wave are $a = 0.2$ and $\omega = 1.0$, respectively. The sloping seabed starts from $x_0 = 7.0$ with a slope of 1:15. The profiles below the free surface illustrate the seabed geometry, which is shifted by $z - 0.5$. The colour bar represents the speed ($|\nabla\phi$) on the free surface).

element method in a time-marching procedure. Compared with the conventional finite element method for water wave problems without involving floating bodies, the QALE-FEM contains two distinctive elements: (1) the scheme for moving the mesh by using a robust spring analogy method purpose-developed for problems associated with oscillating free surfaces and (2) the method for computing velocity on the free surface, which is suitable for unstructured and moving mesh. The main technical developments in this paper are the improvement in these two aspects required for dealing with 3D overturning waves. These include the special techniques for moving the mesh and for calculating the fluid velocity near overturning jets presented in Sections 4 and 5. The main application developments, as discussed in Section 6, include simulations of overturning of solitary waves and transient oscillating waves propagating over 3D complex seabeds. These results reveal some interesting points. For example, overturning jets may be guided to occur in some areas by changing the seabed for engineering purposes; and several overturning jets may simultaneously take place over a complex seabed.

The method has been validated by comparing its numerical predictions with experimental data and results of other numerical methods in many cases with different configurations. This validation leads to the conclusion that the QALE-FEM can yield results agreeing well with experimental data and being at the same level of accuracy as those produced by the BEM. Based on comparison

DOI: 10.1002/fld

with a fast BEM under the same conditions, the QALE-FEM can be over 10 times faster. Using this method, one can obtain the satisfactory results for complex 3D overturning waves within one or two hours on a normal PC. Such efficiency has never been demonstrated by other numerical methods as far as the authors know.

ACKNOWLEDGEMENTS

This work is sponsored by Leverhulme Trust, U.K. (F/00353/G), for which the authors are most grateful.

REFERENCES

1. Wtrwy J. Effects of the 2004 Great Sumatra Tsunami: Southeast Indian. *Journal of Waterway*, *Port*, *Coastal*, *and Ocean Engineering* 2007; **133**:382–400.
2. Black K. Artificial surfing reefs for erosion control and amenity: theory and application. *Proceeding of International Coastal Symposium* (*ICS*), Rotorua, New Zealand, 2000.
3. Wei J, Kirby JT, Grilli ST, Subramanya R. A fully nonlinear Boussinesq model for surface waves. I. Highly nonlinear unsteady waves. *Journal of Fluid Mechanics* 1995; **294**:71–92.
4. Fuhrman DR, Madsen PA. Simulation of nonlinear wave run-up with a high-order Boussinesq model. *Coastal Engineering* 2008; **55**:139–154.
5. Ducrozet G, Bonnefoy F, Le Touzé D, Ferrant P. 3-D HOS simulations of extreme waves in open seas. *Natural Hazards* 2007; **7**:11–14.
6. Ma QW. Numerical generation of freak waves using MLPG_R and QALE-FEM methods. *Computer Modeling in Engineering and Sciences* (*CMES*) 2007; **18**(3):223–234.
7. Miyata H, Kanai A, Kawamura T, Park J. Numerical simulation of three-dimensional breaking waves. *Journal of Marine Science and Technology* 1996; **1**:183–197.
8. Chen G, Kharif C, Zaleski S, Li J. Two-dimensional Navier–Stokes simulation of breaking waves. *Physics of Fluids* 1999; **11**:121–133.
9. Guignard S, Marcer R, Rey V, Kharif C, Fraunie P. Solitary wave breaking on sloping beaches: 2-D two phase flow numerical simulation by SL-VOF method. *European Journal of Mechanics*, *B/Fluids* 2001; **20**(1):57–74.
10. Lubin P, Vincent S, Caltagirone J, Abadie S. Fully three-dimensional direct numerical simulation of a plunging breaker. *Comptes Rendus Mecanique* 2003; **331**(7):495–501.
11. Hieu PD, Katsutoshi T, Ca VT. Numerical simulation of breaking waves using a two-phase flow model. *Applied Mathematical Modelling* 2004; **28**(11):983–1005.
12. Andrillon Y, Alessandrini B. A $2D+T$ VOF fully coupled formulation for the calculation of breaking free-surface flow. *Journal of Marine Science and Technology* 2004; **8**:159–168.
13. Park JC, Kim MH, Miyata H, Chun HH. Fully nonlinear numerical wave tank (NWT) simulations and wave run-up prediction around 3-D structures. *Ocean Engineering* 2003; **30**:1969–1996.
14. Hu C, Kashiwage M. A CIP-based method for numerical simulations of violent free-surface flows. *Journal of Marine Science and Technology* 2004; **9**:143–157.
15. Lo EYM, Shao S. Simulation of near-shore solitary wave mechanics by an incompressible SPH method. *Applied Ocean Research* 2002; **24**(5):275–286.
16. Issa R, Violeau D. Modelling a plunging breaking solitary wave with eddy-viscosity turbulent SPH models. *CMC* 2004; **1**:101–112.
17. Dalrymple RA, Rogers BD. Numerical modelling of water waves with the SPH method. *Coastal Engineering* 2006; **53**:141–147.
18. Koshizuka S, Nobe A, Oka Y. Numerical analysis of breaking waves using the moving particle semi-implicit method. *International Journal for Numerical Methods in Fluids* 1998; **26**:751–769.
19. Gotoh H, Sakai T. Key issues in the particle method for computation of wave breaking. *Coastal Engineering* 2006; **53**:171–179.
20. Pin FD, Idelsohn S, Onate E, Aubry R. The ALE/Lagrangian particle finite element method: a new approach to computation of free-surface flows and fluid-object interactions. *Computers and Fluids* 2007; **36**(1):27–28.
21. Ma QW, Yan S. Quasi ALE finite element method for nonlinear water waves. *Journal of Computational Physics* 2006; **212**:52–72.

DOI: 10.1002/fld

22. Grilli ST, Subramanya R. Numerical modelling of wave breaking induced by fixed or moving boundaries. *Computational Mechanics* 1996; **17**(6):374–391.
23. Skyner DA. A comparison of numerical predictions and experimental measurements of the internal kinematics of a deep-water plunging wave. *Journal of Fluid Mechanics* 1996; **315**:51–64.
24. Yasuda T, Mutsuda H, Mizutani N. Kinematics of overturning solitary waves and their relations to breaker types. *Coastal Engineering* 1997; **29**(3–4):317–346.
25. Yan S. Numerical simulation of nonlinear response of moored floating structures to steep waves. *Ph.D. Thesis*, School of Engineering and Mathematical Sciences, City University, London 2006.
26. Helluy PH, Golay F, Caltagirone JP, Lubin P, Vincent S, Drevard D, Marcer R, Seguin N, Grilli ST, Lesage AC, Dervieux A. Numerical simulations of wave breaking. *Mathematical Modelling and Numerical Analysis* 2005; **39**:591–607.
27. Devrard D, Marcer R, Grilli ST, Fraunie P, Rey V. Experimental validation of a coupled BEM-Navier–Stokes model for solitary wave shoaling and breaking. *Proceeding of 5th International Symposium on Ocean Wave Measurement and Analysis*, Madrid, Spain, 2005; 166–176.
28. Grilli ST, Guyenne P, Dias F. A fully non-linear model for three-dimensional overturning waves over an arbitrary bottom. *International Journal for Numerical Methods in Fluids* 2001; **35**(7):829–867.
29. Lachaume C, Biausser B, Grilli ST, Fraunie P, Guignard S. Modelling of breaking and post-breaking waves on slopes by coupling of BEM and VOF methods. *Proceedings of the International Offshore and Polar Engineering Conference*, Honolulu, HI, U.S.A., 2003; 1698–1704.
30. Garzon M, Sethian JA. Wave breaking over sloping beaches using a coupled boundary integral-level set method. *International Series of Numerical Mathematics* 2006; **154**:189–198.
31. Longuet-higgins MS, Cokelet ED. The deformation of steep waves on water: I. A numerical method of computation. *Proceedings of the Royal Society of London*, *Series A* 1976; **350**:1–26.
32. Dommermuth DG, Yue DKP, Lin WM, Rapp RJ, Chan ES, Melville WK. Deep water plunging breakers: a comparison between potential theory and experiments. *Journal of Fluid Mechanics* 1988; **189**:423–442.
33. Vinje T, Brevig P. Numerical simulation of breaking waves. *Advances in Water Resources* 1981; **4**(2):77–82.
34. New AL, Mciver P, Peregrine DH. Computation of overturning waves. *Journal of Fluid Mechanics* 1985; **150**:233–251.
35. Grilli ST, Skourup J, Svendsen IA. An efficient boundary element method for nonlinear water waves. *Engineering Analysis with Boundary Elements* 1989; **6**:97–107.
36. Seo SN, Dalrymple RA. An efficient model for periodic overturning waves. *Engineering Analysis with Boundary Elements* 1990; **7**:196–204.
37. Cooker MJ, Peregrine DH. Violent water motion at breaking-wave impact. *Proceedings of the Coastal Engineering Conference*, Delft, The Netherlands, vol. 1, 1990; 164–176.
38. Otta AK, Svendsen LA, Grilli ST. The breaking and run-up of solitary waves on beaches. *Proceedings of the Coastal Engineering Conference*, Venice, Italy, vol. 2, 1992; 1461–1474.
39. Cao Y, Beck RF, Schultz WW. Numerical computations of two-dimensional solitary waves generated by moving disturbances. *International Journal for Numerical Methods in Fluids* 1993; **17**(10):905–920.
40. Wang P, Yao Y, Tulin MP. Wave group evolution, wave deformation, and breaking: simulations using LONGTANK, a numerical wave tank. *International Journal of Offshore and Polar Engineering* 1994; **4**(3):200–205.
41. Grilli ST, Svendsen IA, Subramanya R. Breaking criterion and characteristics for solitary waves on slopes. *Journal of Waterway*, *Port*, *Coastal and Ocean Engineering* 1997; **123**:102–112.
42. Maiti S, Sen D. Computation of solitary waves during propagation and runup on a slope. *Ocean Engineering* 1999; **26**(11):1063–1083.
43. Grilli ST, Gilbert R, Lubin P, Vicent S, Legendre D, Duyam M, Kimmoun O, Branger H, Devrard D, Fraunie P, Abadie S. Numerical modeling and experiments for solitary wave shoaling and breaking over a sloping beach. *Proceedings of the Fourteenth* (*2004*) *International Offshore and Polar Engineering Conference* (*ISOPE2004*), Toulon, France, 2004; 306–312.
44. Drimer N, Agnon Y. An improved low-order boundary element method for breaking surface waves. *Wave Motion* 2006; **43**(3):241–258.
45. Christou M, Swan C, Gudmestad OT. The description of breaking waves and the underlying water particle kinematics. *The International Conference on Offshore Mechanics and Arctic Engineering* (*OMAE2007*), San Diego, U.S.A., 2007; 291–299.
46. Ortiz JC, Douglass SL. Boundary element solution of water particle velocities of waves breaking on mild slopes. *Boundary Element XV*: *Fluid Flow and Computational Aspects*, Worcester Polytechnic Institute, Worcester, MA. Computational Mechanics, 1993; 221–232. ISBN: 1562521977 9781562521974.

47. Zhao R, Faltinsen OM. Water entry of a two-dimensional body. *Proceedings of 6th International Workshop on Water Waves and Floating Bodies*, Woods Hole, MA, U.S.A., 1991; 275–279.
48. Xü H, Yue DKP. Numerical study of three dimensional overturning waves. *Proceedings of 7th International Workshop on Water Waves and Floating Bodies*, Cointe, France, 1992; 303–307.
49. Xü H, Yue DKP. Numerical study of kinematics of nonlinear water waves in three dimensions. *Civil Engineering in the Oceans V*, 1992; 81–98.
50. Xue M, Xü H, Liu Y, Yue DKP. Computations of fully nonlinear three-dimensional wave-wave and wave-body interactions. Part 1. Dynamics of steep three-dimensional waves. *Journal of Fluid Mechanics* 2001; **438**:11–39.
51. Guyenne P, Grilli ST. Numerical study of three-dimensional overturning waves in shallow water. *Journal of Fluid Mechanics* 2006; **547**:361–388.
52. Grilli ST, Vogelmann S, Watts P. Development of a 3D Numerical Wave Tank for modelling tsunami generation by underwater landslides. *Engineering Analysis with Boundary Elements* 2002; **26**(4):301–313.
53. Brandini C, Grilli ST. Modeling of freak wave generation in a 3D-NWT. *Proceedings of the International Offshore and Polar Engineering Conference* (*ISOPE2001*), vol. 3, Stavanger, Norway 2001; 124–131.
54. Fochesato C, Dias F. A fast method for nonlinear three-dimensional free-surface waves. *Proceedings of the Royal Society of London*, *Series A* 2006; **462**:2715–2735.
55. Fochesato C, Grilli ST, Dias F. Numerical modelling of extreme rogue waves generated by directional energy focusing. *Wave Motion* 2007; **44**(5):395–416.
56. Wu GX, Eatock Taylor R. Finite element analysis of two dimensional non-linear transient water waves. *Applied Ocean Research* 1994; **16**:363–372.
57. Ma QW, Wu GX, Eatock Taylor R. Finite element simulation of fully non-linear interaction between vertical cylinders and steep waves. Part 1: methodology and numerical procedure. *International Journal for Numerical Methods in Fluids* 2001; **36**(3):265–285.
58. Ma QW, Wu GX, Eatock Taylor R. Finite element simulation of fully non-linear interaction between vertical cylinders and steep waves. Part 2: numerical results and validation. *International Journal for Numerical Methods in Fluids* 2001; **36**(3):287–308.
59. Turnbull MS, Borthwick AGL, Eatock Taylor R. Wave–structure interaction using coupled structured–unstructured finite element meshes. *Applied Ocean Research* 2003; **25**:63–77.
60. Heinze C. Nonlinear hydrodynamic effects on fixed and oscillating structures in waves. *Ph.D. Thesis*, Department of Engineering Science, Oxford University, 2003.
61. Wang CZ, Wu GX. An unstructured-mesh-based finite element simulations with non-wall-sided bodies. *Journal of Fluids and Structures* 2006; **22**:441–461.
62. Wang CZ, Wu GX, Drake KR. Interactions between nonlinear water waves and non-wall-sided 3D structures. *Ocean Engineering* 2007; **34**:1182–1196.
63. Westhuis JH, Andonowati AJ. Applying the finite element method in numerically solving the two dimensional free-surface water wave equations. *Proceedings of the 13th International Workshop on Water Waves and Floating Bodies*, Hermans, The Netherlands, 1998; 171–174.
64. Clauss GF, Steinhagen U. Numerical simulation of nonlinear transient waves and its validation by laboratory data. *Proceedings of the International Offshore and Polar Engineering Conference* (*ISOPE1999*), vol. 3, Brest, France, 1999; 368–375.
65. Wu GX, Hu ZZ. Simulation of nonlinear interactions between waves and floating bodies through a finite-element-based numerical tank. *Proceedings of the Royal Society of London*, *Series A* 2004; **460**:3037–3058.
66. Sriram V, Sannasiraj SA, Sundar V. Simulation of 2-D nonlinear waves using finite element method with cubic spline approximation. *Journal of Fluids and Structures* 2006; **22**:663–681.
67. Yan S, Ma QW. Application of QALE-FEM to the interaction between nonlinear water waves and periodic bars on the bottom. *Proceedings of the 20th International Workshop on Water Waves and Floating Bodies*, Norway, 2005.
68. Ma QW, Yan S. QALE-FEM for numerical modelling of nonlinear interaction between 3D moored floating bodies and steep waves. *International Journal for Numerical Methods in Engineering* 2009; **78**:713–756.
69. Yan S, Ma QW. Numerical simulation of fully nonlinear interaction between steep waves and 2D floating bodies using the QALE-FEM method. *Journal of Computational Physics* 2007; **221**:666–692.
70. Yan S, Ma QW. Effects of an arbitrary sea bed on responses of moored floating structures to steep waves. *Proceedings of the Seventeenth International Offshore and Polar Engineering Conference* (*ISOPE2007*), Lisbon, Portugal, 2007; 2192–2199.

DOI: 10.1002/fld

71. Frey PJ, Borouchaki H, George P. 3D Delaunay mesh generation coupled with an advancing-front approach. *Computer Methods in Applied Mechanics and Engineering* 1998; **158**:115–131.
72. Farhat C, Degand C, Koobus BM, Lesoinne M. A three-dimensional torsional spring analogy method for unstructured dynamic meshes. *Computers and Structures* 2002; **80**:305–316.
73. Bottasso CL, Detomi D, Serra R. The ball-vertex method: a new simple spring analogy method for unstructured dynamic meshes. *Computer Methods in Applied Mechanics and Engineering* 2005; **194**:4244–4264.
74. Zeng D, Ethier CR. A semi-torsional spring analogy model for updating unstructured meshes in 3D moving domains. *Finite Elements in Analysis and Design* 2005; **41**:1118–1139.
75. Lewis RW, Zheng Y, Gethin DT. Three-dimensional unstructured mesh generation: part 3. Volume meshes. *Computer Methods in Applied Mechanics and Engineering* 1996; **134**:285–310.
76. Tanaka M. The stability of solitary waves. *Physics of Fluids* 1986; **29**:650–655.
77. Kimmoun O, Branger H, Zucchini B. Laboratory PIV measurements of wave breaking on a beach. *The Fourteenth* (*2004*) *International Offshore and Polar Engineering Conference* (*ISOPE*), Toulon, France, 2004; 293–298.

DOI: 10.1002/fld